# Understanding the Surface Chemistry of Thiolate-Protected Metallic Nanoparticles

Julio C. Azcárate,[†,⊥] Gastón Corthey,[†,#,⊥] Evangelina Pensa,[†] Carolina Vericat,[†] Mariano H. Fonticelli,[†] Roberto C. Salvarezza,*[,†] and Pilar Carro[§]

[†]Instituto de Investigaciones Fisicoquímicas Teóricas y Aplicadas (INIFTA), Facultad de Ciencias Exactas, Universidad Nacional de La Plata - CONICET, Sucursal 4 Casilla de Correo 16, 1900 La Plata, Argentina

[§]Departamento de Química Física, Instituto de Materiales y Nanotecnología, Universidad de La Laguna, Avda. Astrofísico Francisco Sánchez S/N, La Laguna 38071, Tenerife, Spain

ABSTRACT: Metallic nanoparticles (NPs) appear as promising materials to be used in biomedicine, as efficient catalysts and electrocatalysts, and as active elements in electronic and sensing devices. The most common strategy to protect these NPs is by using thiolate self-assembled monolayers (SAMs), a strategy that has proved to be useful to control the physical and chemical properties of extended solid surfaces. However, the knowledge of the structure and chemistry of thiol−metal interfaces yet remains elusive, although it is crucial for understanding how NPs interact with molecules, biomolecules, and living cells and also for a better design of NP-based devices. This Perspective strives to show the complexity of the thiol−metal NP interface chemistry and how this changes with the nature of the metallic core.
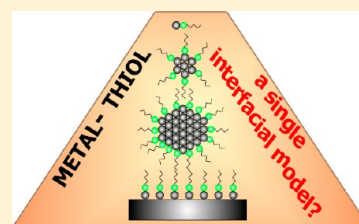
The use of metallic nanoparticles (NPs) for biomedical applications, as efficient catalysts and electrocatalysts, and for the development of NP-based devices, among others, has been of the main interest of the scientific community working in nanoscience and nanotechnology.[1−4]

Synthesis of NPs often requires the use of ligands that control nucleation and growth and provide chemical and colloidal stability.[5] Thiols are the most popular ligands because they adsorb as thiolates, forming self-assembled monolayers (SAMs) on the NP surface. This strategy has proved to be useful to control the physical and chemical properties of extended solid surfaces.[6] Thiolates protect the NP metallic core, hinder aggregation, and promote ordered particle assembling on surfaces due to the strong sulfur head−metal covalent bonding and the intermolecular interactions. Moreover, thiol terminal groups (at the molecule/environment interface) and S heads (at the molecule/metal interface) determine most of the physicochemical properties and the reactivity of the NPs.[7] While the outer interface is more accessible to experimental techniques and thus is better understood, the spatial structure and chemistry of the buried S head/metal interface remain today a challenge for the scientific community. This knowledge is crucial for understanding how NPs interact with molecules, biomolecules, and cells and also for the behavior of NP-based devices.

This Perspective strives to show the complexity of the thiol/metal NP interface chemistry and how this complexity changes with the nature of the metallic core. We will focus our analysis on thiolate-protected Au, Ag, and Pd NPs, which have shown to be examples of metals with very different chemical reactivity.

Synthesis of Thiolate-Protected Metallic NPs. The Brust−Schiffrin syntheses in one[8] (BS-I) and two (BS-II) phases[9] remain the preferred methods to prepare either hydrophilic or hydrophobic

> The fact that thiolates are produced after the formation of the metallic cores creates some link between the two-phase Brust−Schiffrin method and ligand exchange reactions. Under certain conditions, some metal thiolate polymers are very stable in polar media, and incomplete reduction of these species can occur.

thiolate-protected metallic NPs, respectively, both with a relatively high monodispersity and a mean size controllable by the thiol/metal molar ratio.

There is a large amount of work on the BS-II method to synthesize hydrophobic thiolate-protected NPs including Au,[9] Ag,[10] Cu,[11] Pd,[12] and Pt[13] (Figure 1). In the case of AuNPs, Au(III) is first transferred to a toluene phase using quaternary ammonium salts (NR_4X). The aqueous phase is discarded, and thiols are added to the organic phase, which reduce Au(III) to Au(I) species. Early, it was believed that insoluble Au(I)-thiolate polymeric species ($[Au(I)-SR]_n$) were formed during this reaction.[14] However, these cannot be considered the only possible precursors.[15] In fact, recent results have shown that ion pairs of tetraalkylammoniun and Au(I)-halide complexes
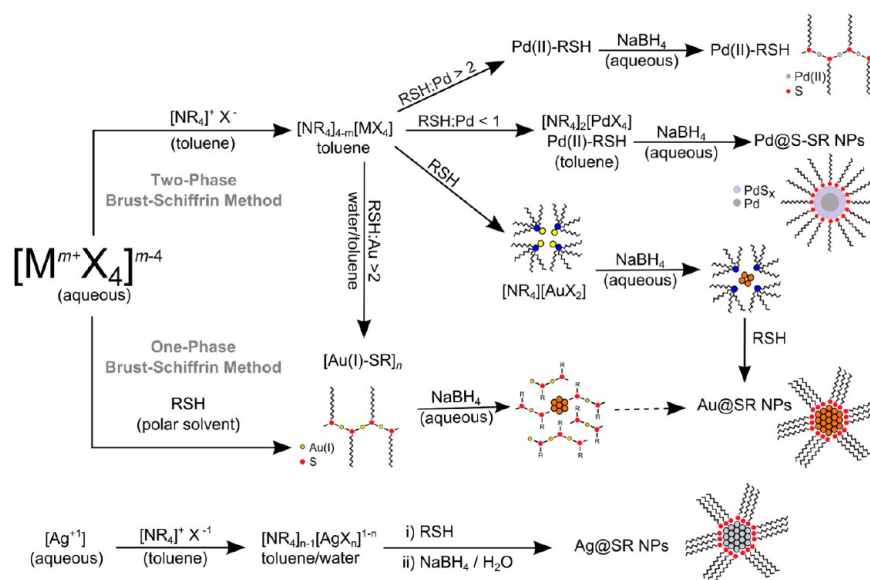
Figure 1. Scheme showing synthetic routes of thiolate-capped Au, Pd, and Ag NPs.

($[NR_4][AuX_2]$) are the real intermediates.[16] There is evidence that Au(I) species are encapsulated into inverse micelles of tetraalkylammonium cations.[11] Also, if the aqueous phase is left in the reaction media during the addition of thiol and the thiol/metal molar ratio is ≥2, the reaction intermediates will consist of a mixture of $[NR_4][AuX_2]$ and $[Au(I)\text{-}SR]_n$ species. Reduction of Au(I) species to Au(0) clusters is accomplished by a strong reducing agent, such as $NaBH_4$ in aqueous solution. Finally, thiol molecules in toluene bind to the metallic cluster, leading to thiolate-protected NPs.

Similar reaction schemes are applicable to the synthesis of AgNPs,[17] although some drawbacks should be considered, like the possible formation of AgBr precipitates. In the case of PdNPs the metal halide complexes $[PdX_4]^{2-}$ (X = Br, Cl) are inside of the inverse micelles containing Pd(II)-thiol complexes.[12] Both Pd(II)-thiol and $[PdX_4]^{2-}$ species can be reduced to metallic Pd clusters when the thiol/metal molar ratio is <1[18] (Figure 1). For higher molar ratios, incomplete or negligible reduction of the metallic species is observed. Also, Pt(II)-thiol complexes could not be reduced upon addition of $NaBH_4$ when a 2/1 thiol/metal molar ratio was used.[13] This issue was overcome by inverting the reactant addition sequence.

The fact that metal−sulfur bonds are produced after the formation of the metallic cores allows linking of the BS-II method with ligand exchange reactions, where weak bond-capping agents are replaced by thiols.[16] If the amount of thiol is relatively small and the reaction time is short, thiolate-protected NPs are obtained, while at high thiol concentration, smaller NPs are formed due to digestive ripening.[19,20]

The BS-I method[8] (Figure 1) is used to prepare hydrophilic thiolate-protected NPs, although there are some examples of hydrophobic NPs.[21] In the case of AuNPs, Au(III) ions are first reduced to Au(I) upon addition of thiols in polar media (tetrahydrofuran, methanol), which leads to the formation of $[Au(I)\text{-}SR]_n$. These polymeric species are further reduced by $NaBH_4$ or $LiEt_3BH$ to obtain thiolate monolayer-protected NPs. In a similar way, PdNPs[22] and AgNPs[21] have been synthesized. However, under certain conditions, some metal thiolate polymers are very stable in polar media, and incomplete reduction of these species can occur.[23] For instance,

the existence of a $[Au(I)\text{-}SR]_n$ shell with a ~1 nm Au(0) core has been reported for a typical reaction using thiomalic acid (TMA).[24] Moreover, TMA-protected PtNPs prepared by this method[25] and subsequent etching with glutathione exhibit a large amount of oxidized Pt species, suggesting also the formation of a $[Pt(I)\text{-}SR]_n$ shell. Also, during the synthesis of dodecanethiolate (DT)-protected NiNPs, the reduction of $NiCl_2$ with $NaBH_4$ in the presence of DT yields $[Ni(II)\text{-}SR]_n$ species surrounding Ni(0) clusters ~1 nm in size.[26,27]

The Brust−Schiffrin route is very effective in the synthesis of NPs less than 5.0 nm. On the other hand, alkylthiosulfates have been used to prepare thiolated-protected NPs 5−20 nm in size by direct aqueous synthesis in the presence of $NaBH_4$.[28−30]

In a simplified outline, synthetic routes can result in two different types of NPs, thiolate monolayer-protected NPs and metal thiolate polymer-coated NPs. The latter is frequently found for the one-phase method when reduction of the metal thiolate produced by the metal precursor in the polar media is difficult. On the other hand, the BS-II and ligand exchange methods, where the thiol molecules chemisorb on the metallic clusters covered by weakly adsorbed species, can be better compared with thiol self-assembly on extended metal surfaces.

Structure and Shape of Clean Metallic NPs. It is well-known that surface energy considerations are crucial to understand and predict the morphology of noble metal NPs.[31] Surface energy (γ), defined as the excess free energy per unit area for a particular crystallographic face, largely determines the faceting and crystal growth observed for particles at the nanoscale. Noble metals, with a face-centered cubic (fcc) lattice, have different γ's for different crystal planes.[32] The anisotropy results in stable morphologies where γ is minimized by the low-index crystal planes that exhibit closest atomic packing. For Au, Ag, Cu, Ni, Pd, and Pt at $T = 0$ K, surface energy calculations predict that any high-index crystal planes will spontaneously facet into linear combinations of the low-index {111}, {100}, and {110} planes.[33] Each crystal facet possesses a different γ value, being $\gamma\{111\} < \gamma\{100\} < \gamma\{110\}$.

The predicted thermodynamic equilibrium shape of mono-crystalline NPs 3−100 nm in size at $T = 0$ K is a truncated octahedron bound by {111} and {100} planes with 90% {111}
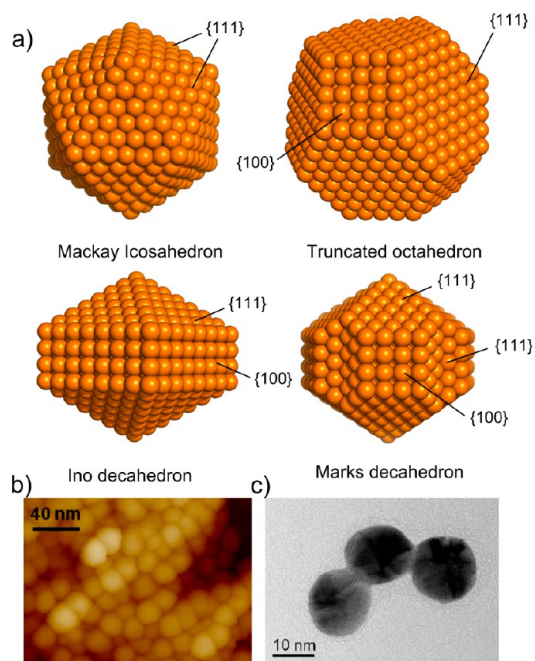
Figure 2. (a) Some of the shapes exhibited by NPs. The different facets are indicated; (b) scanning tunneling microscopy (STM) and (c) transmission electron microscopy (TEM) images of citrate-coated AuNPs. (TEM image taken by M. S. Moreno, CAB-CNEA.) Faceted and "spherical"-looking NPs are shown.

and 10% {100} surface areas (Figure 2).[34] Even the most "spherical"-looking NPs may be described by a truncated octahedron. However, as NPs become smaller, not only does the fraction of surface sites increase, but also their shape transforms into decahedra or icosahedra, the latter exclusively formed by the {111} fcc crystal planes (Figure 2).[35] Due to accumulated strain energy, the stability of the icosahedral forms decreases significantly as the cluster size is increased.[36] Thus, the AuNPs stability map at T = 300 K predicts icosahedra– decahedra and decahedra–truncated octahedra transitions at ~10 and ~14 nm NP sizes, respectively, with 77% {111} and 23% {100} surface areas.[35] Also, theoretical modeling of PdNPs at 300 K has shown that decahedral–truncated octahedral shape transition takes place at ~10 nm.[37] Similar transitions have been observed for AgNPs.[38] However, some of the most common particle morphologies are not composed of single domains but rather possess multiply twinned planes (MTPs).[32] The formation of MTPs for Au, Ag, Cu, Pd, and Pt results from their small twinning energy, which accommodates the strain induced by a completely (111)-bound particle.[32] Only at low temperature and small sizes are multiply twinned decahedra stable; monocrystalline shapes are thermodynamically preferred under most conditions.[37]

Decahedral and icosahedral NPs have been observed at sizes that defy predictions made by theory, suggesting other stabilization mechanisms. These involve the formation of high-index {511} facets and reconstruction of {001} faces.[39] The former possess a high density of low-coordinated atoms, steps, edges, and kinks,[40] and because of their high γ, they should vanish faster at a crystal growth stage and are more difficult to be preserved on the surface of the final NPs.

Metallic NPs exhibit a lattice contraction as their size decreases below 4 nm, resulting in lattice parameters smaller than those of the bulk metal.[41−43] In fact, the coordination

number loss in the NP surface leads to bond contraction at the surface and subsurface due to surface tension effects.[44] In the case of AuNPs[44] and PtNPs, a 4−5% bond contraction has been calculated.[45] The high surface free energy of NPs < 4 nm results in high evaporation rates, high adatom mobility, and low melting temperature.[46]

The above picture of NPs results from theoretical calculations for pristine NPs and from experimental data for NPs protected by weakly adsorbed species. Next, we will discuss the chemistry and structure of thiols on (111) and (100) metal surfaces.

Thiol Self-Assembly on (111) and (100) Crystal Faces. Thiol-protected NPs can be considered as a metallic core with a complex thiolate−metal shell. If the size of the metallic core is large, the NP interface properties approximate to those of SAMs on planar surfaces. If the metal cluster size is reduced enough, then all of the metal atoms in the cluster are directly bonded to the S head, and the system approaches a metal thiolate. Next, we will briefly discuss the present knowledge of thiolate SAMs on (111) and (100) surfaces because they dominate NP surfaces.

Thiols adsorb on Au(111) and Au(100) single-crystal surfaces, forming strong (2−3 eV) covalent S−Au bonds (thiolates, RS). The stable phases on Au(111) at high coverage are the $(\sqrt{3} \times \sqrt{3})$-R30° and c(4 × 2) lattices that coexist on the substrate, with the $(\sqrt{3} \times \sqrt{3})$-R30°/c(4 × 2) ratio increasing with hydrocarbon chain length.[47] Exceptions are methanethiol (MT) and ethanethiol (ET), which arrange into a (3 × 4) lattice.[48] In all cases, the surface coverage on the Au(111) face is θ = 0.33, the nearest-neighbor thiol−thiol distances is $d \approx 0.5$ nm, and the tilt angle of the hydrocarbon chain with respect to the substrate normal (α) is ~30°.[47] The initial picture of adsorbed RS on an unreconstructed (U) Au(111) surface has been replaced by models involving gold adatom (Au$_{ad}$)-RS complexes with a considerable substrate reconstruction.[49]

The most accepted models[47] involve RS-Au$_{ad}$-SR ("staple") units based on scanning tunneling microscopy (STM) results at low[50] and high[48] θ values. Recent data[48] for MT and ET at high θ give direct evidence of RS-Au$_{ad}$-SR species in the trans configuration ((3 × 4) lattice) (Figure 3a), while the cis configuration (c(4 × 2) lattice) (Figure 3b) is more stable for longer thiols.[47,49] Also, RS-Au$_{ad}$-(RS)-Au$_{ad}$-RS and RS-Au$_{ad}$ have been found as intermediate species at low θ.[51]

Generally, strong electronegative adsorbates can release gold from the surface. Thus, the uptake of Au$_{ad}$ to form RS-Au$_{ad}$-SR species results in a single vacancy,[49,52] which can either diffuse to form vacancy islands on terraces (see the black holes in Figure 4a) or be adsorbed at step edges (see the serrated steps in Figure 4b).

Figure 4c shows the calculated Gibbs free energy for single vacancy formation on clean and thiol-covered U Au(111) substrates.[53] It is evident that upon thiol chemisorption, the uptake process becomes thermodynamically favored not only along step-edge lines and strained surfaces but also at (111) terraces. The ability of thiols to extract Au atoms is demonstrated in Figure 4d−f, where butanethiol (BT) adsorption leads to a separation of the Au atom from the step edge. The absence of vacancy islands on 5 nm wide terraces (Figure 4b) indicates that the mean free path of diffusing vacancies is larger and therefore that they can be captured at steps before they create a new island. The absence of vacancy islands after adsorption of some aromatic thiols
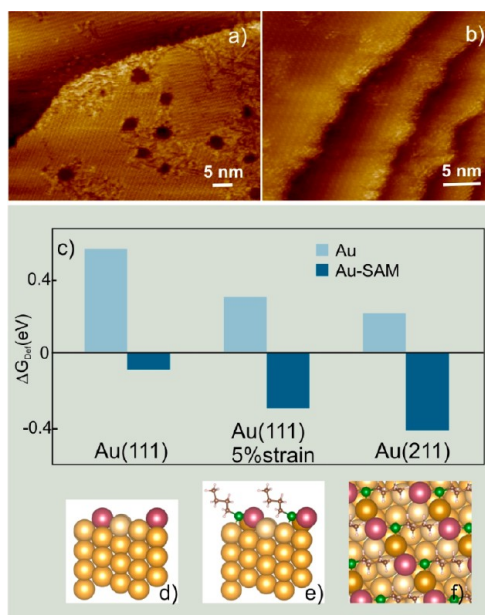
3129

dx.doi.org/10.1021/jz401526y | J. Phys. Chem. Lett. 2013, 4, 3127−3138
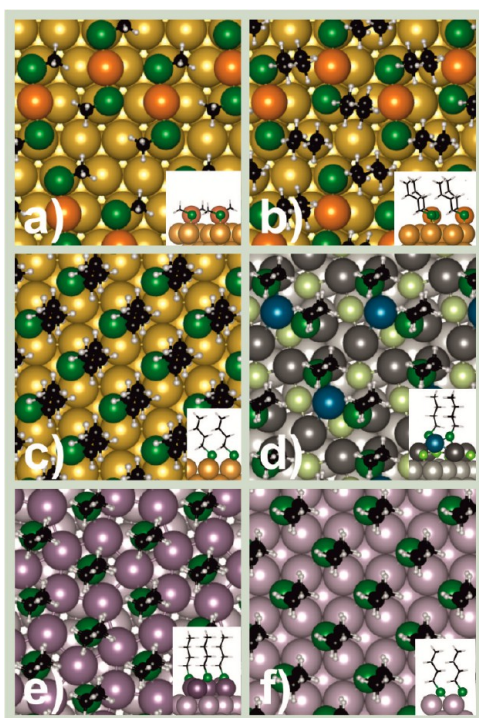
Figure 3. Optimized structures for alkanethiols on different metal surfaces: (a) MT "staple" (3 × 4) model on Au(111), (b) butanethiol (BT) "staple" c(4 × 2) model on Au(111), (c) BT on unreconstructed Au(100), (d) BT "staple" on S covered-Pd(111), (e) BT on a 5/7 model on Ag(111), and (f) BT on unreconstructed Ag(100). Insets: lateral view of the structures. Gold: Au; gray: Pd; violet: Ag; green: S-thiolate; light-green: S-sulfide; black: C; white: H. (a,b) Orange: Au adatoms; (d) blue: Pd adatoms.

Figure 4. (a) STM images showing hexanethiol (HT) c(4 × 2) domains on Au(111). Black holes represent vacancy islands. (b) HT-covered terraces 5−10 nm in width showing the absence of vacancy islands and serrated steps. (c) Vacancy-formation Gibbs free energies, ΔG_{Def}, for a set of different Au motifs in the absence (light blue) and in the presence (blue) of an adsorbed MT SAM: (left) Au(111), (center) Au(111) under uniaxial 5% compressive strain, and (right) Au(211) stepped surface (taken from ref 53). (d) Clean stepped Au(211). (e) Lateral view and (f) top view after BT adsorption at step edges. Note that the Au atom bonded to the BT is elevated.

(Figure 5a,b) suggests that staple formation on the Au(111) is more difficult for these thiols.

In the case of 4-mercaptobenzoic acid (MBA) on Au(111), a diluted (4 × √3) lattice was observed (inset in Figure 5a and Figure 5d).[54] The γ versus adsorbate chemical potential ($\Delta\mu$) plot (Figure 5c) shows that at low $\Delta\mu$ values, this lattice is more stable than a c(4 × 2) lattice containing RS-Au$_{ad}$-SR species (Figure 5e), thus explaining the experimental data. The absence of reconstruction has been observed for other aromatic thiols, such as 6-mercaptopurine (6MP) (Figure 5f),[55] which also exhibits a dilute lattice (Figure 5b, inset). The low binding energy (E_b) and the low Bader charge (q) on the Au atom (small repulsion at the surface) could explain why these molecules fail to reconstruct the Au(111) terraces.

Unlike Au(111), the adsorption of thiol molecules on a Au(100) has been less studied. Short-chain alkanethiols form a c(2 × 2) overlayer with d = 0.41 nm, θ = 0.5, and $\alpha \approx 30°$ (Figure 3c).[56] On the other hand, STM images in solution show that ET organizes in a quadratic incommensurate lattice with d = 0.44 nm and θ = 0.43.[57] These images also show a 0.25 Au island coverage, a figure consistent with the lifting of the hexagonal reconstruction of the Au(100) surface to form the Au(1 × 1) surface. This fact suggests that the thiol-covered (100) surface is unreconstructed. Longer-chain homologues, however, show more complex diffraction patterns.[56]

SAMs on Pd(111) have also been characterized by using different techniques.[58,59] Thiol molecules on this surface adopt a standing-up configuration with $\alpha \approx 14−18°$.[58] A careful analysis of X-ray photoelectron spectroscopy (XPS) data shows that thiols adsorb on Pd at saturation coverage, forming a complex interface that consists of thiolates on a diluted palladium sulfide (PdS$_x$) with $\theta_{sulfide} \approx 0.4$ and $\theta \approx 0.30$ (total S coverage $\theta_S \approx 0.7$).[59] This complex adlayer has been modeled as a (√7 × √7)R19.1° S + thiol ($\theta_{sulfide}$ = 3/7 + $\theta_{thiolate}$ = 2/7) lattice[60] (Figure 3d). The presence of sulfide reflects the ability of metals with d-bands populated near the Fermi level to break bonds of the adsorbates. Upon thiol adsorption on Pd, there is an electron density transfer from the metal d-band to the antibonding molecular orbitals of thiol molecules that weakens the S−C bond, resulting in its elongation and final breakage. In fact, after S adsorption, the center of the d-band is lowered in energy with respect to the clean surface, that is, the surface is "passivated", allowing thiol adsorption and SAM formation. In contrast, significant amounts of atomic S on Au(111) are only observed in the adsorption of some small thiol molecules from the liquid phase.[61−64] In these cases, S adlayers result from S−C bond scission or thiol decomposition in solution. DFT calculations also show that thiol adsorption on the PdS$_x$ surface is able to extract Pd atoms from the surface, forming RS-Pd$_{ad}$-SR moieties (inset in Figure 3d) similar to those found on thiol-covered Au(111).[60] This is reasonable as aliphatic and aromatic complexes forming [Pd(SR)$_2$]$_n$ polymers have been prepared.[65]

It is well-known that thiols adsorb on Ag(111) as thiolates in a distorted (√7 × √7)R19.1° lattice ($\theta \approx 0.43$) of standing-up molecules with $\alpha \approx 0−19°$[66,67] However, experimental data from different techniques have excluded any simple adsorption model on an unreconstructed Ag(111) surface.[68] Therefore, it has been proposed that Ag(111) reconstructs, forming a near-hexagonal surface layer with a Ag density that is only 3/7 that
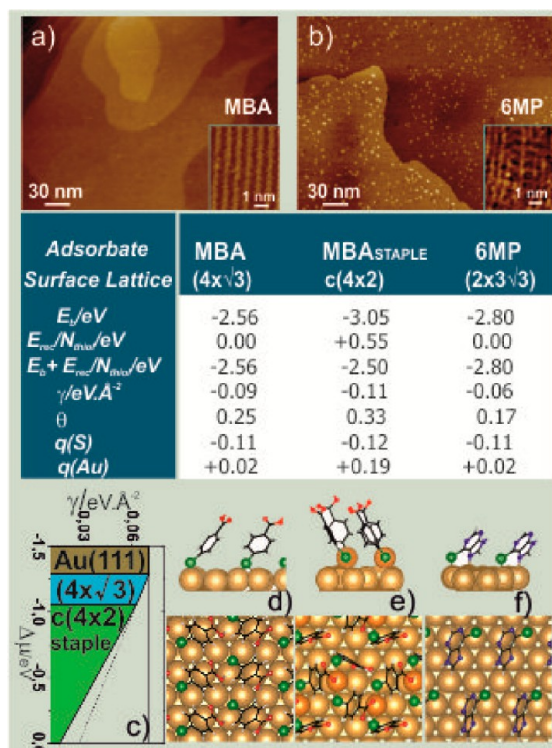
Figure 5. STM images of (a) MBA and (b) 6MP SAMs on Au(111). High-resolution images for these SAMs are shown in the insets. Binding energies (E_b), the reconstruction energy per thiol (E_{rec}/N_{thiol}), the surface free energy (γ), the surface coverage by sulfur species (θ_S), and Bader charges on the S and metal atoms (q) from DFT calculations (optB88-including van der Waals interactions) are listed for different aromatic thiol lattices on Au(111). (c) γ versus $\Delta\mu$ of MBA (from disulfide). The stability of the different surfaces is shown. (d) MBA ($4 \times \sqrt{3}$), (e) MBA staple $c(4 \times 2)$, and (f) 6MP ($2 \times 3\sqrt{3}$).

of the underlying substrate layers with MT molecules adsorbed into three-fold-coordinated hollow sites with d = 0.44 nm.[69] However, the stability of this model is similar to that of the $(\sqrt{7} \times \sqrt{7})R19.1°$ MT lattice on the U surface as the formation of Ag vacancies implies a large energy cost.[70] More recently, a DFT study has proposed a more stable structure for MT involving a greater density (5/7) of topmost Ag atoms.[71] The adsorption pattern consists of $Ag_3(MT)_3$ units surrounded by hexagons of Ag atoms. For alkanethiols longer than MT, the same reconstructed model (Figure 3e) seems to be valid,

although d increases to ~0.47 nm in order to optimize hydrocarbon chain interactions.[68,72] Concerning thiolate–Ag complexes, Ag(SR) species arranged in a planar lamellar shape are preferentially formed.[73] On the other hand, it has been reported that thiols remain intact on Ag(111) from the gas phase at room temperature,[74] although exposure to UV radiation[75] or thermal desorption at high temperature[74] causes C–S bond scission and the formation of S-rich Ag surfaces. Much less information can be found for thiol adsorption on the Ag(100) face. Here, thiolates adsorb in four-fold hollow sites by the S atoms[76] (Figure 3f).

Several energetic and structural parameters for BT adsorption on different Au, Ag, and Pd substrates are shown in Table 1. The E_b and γ data indicate that the reconstructed (111) surface models exhibit enhanced adsorption and are more stable than that on the U (111) surface, thus supporting experimental observations. Interestingly, the $c(2 \times 2)$ BT lattice on the unreconstructed Au(100) and Ag(100) surfaces has large E_b and high stability in terms of γ, suggesting that these surfaces are not reconstructed upon thiol adsorption.[57] Bader charges show that the intrinsic dipole in the S–Au bond is quite small, whereas S–Ag and S–Pd bonds have a strong polar character.[59,77]

Chemistry of the Thiolate-Protected Metallic Nanoclusters. Noble metal nanoclusters (NCs, diameter < 2 nm) have been the focus of increasing research interest because they exhibit unique properties compared to NPs (diameter > 2 nm) such as fluorescence,[79] chirality,[80] or magnetism.[81] Therefore, they have promising applications in the fields of catalysis,[82] sensing,[83] photonics,[84] or biolabeling.[85]

> Surface reconstruction of {111} nanoparticle facets upon thiol adsorption is enhanced in relation to that of plain surfaces due to bond contraction and a large number of defects, both favoring vacancy and adatom formation.

Today, it is possible to synthesize thermodynamically stable thiolate-protected AuNCs of the formula $Au_m(SR)_n$, with m = 24, 25, 38, 102, 130, 144, and 225.[19] A key point in the present understanding of the surface chemistry of the S/Au interface

Table 1. Energetic and Structural Data and Bader Charges from DFT Calculations (optB88-vdW) for BT Adsorption on Reconstructed (R) Au(111), Ag(111), and Pd(111) Surfaces According to the Models Reported in References 78, 60, and 71, respectively[a]

	Au(111) R_{staple}	Au(111) U	Au(100) U	Ag(111) R	Ag(111) U	Ag(100) U	Pd(111) R	Pd(111) U
lattice	$c(4 \times 2)$	$c(4 \times 2)$	$c(2 \times 2)$	$(\sqrt{7} \times \sqrt{7})R19.1°$	$(\sqrt{7} \times \sqrt{7})R19.1°$	$c(2 \times 2)$	$(\sqrt{7} \times \sqrt{7})R19.1°$	$(\sqrt{3} \times \sqrt{3})R30°$
E_b /eV	−3.28	−2.26	−2.84	−3.18	−2.53	−2.75	−3.18	−3.32
(E_{rec}/N_{thiol})/eV	+0.51	0	0	+0.51	0	0	−2.32[c]	0
γ/ eV·Å^{-2}	−0.123	−0.100	−0.164	−0.154	−0.146	−0.160	−0.236	−0.166
θ_S	0.33	0.33	0.50	0.43	0.43	0.5	0.7	0.33
α/deg	34	10.0	23.8	4.21	6.1	8.3	3–9	11.1
$q(S)$	−0.18	−0.23	−0.17	−0.37	−0.39	−0.39	−0.37/−0.23	−0.24
$q(Me)$	+0.14[b]	+0.06	+0.06	+0.22	+0.13	+0.16	+0.26[b]	+0.07

[a]Data are compared to those found for BT on unreconstructed surfaces (U). Parameters for adsorption on the Au(100) and Ag(100) surfaces are also included. [b]Charge on the Au adatom. [c]Include the energy to reconstruct the sulfide–Pd surface with respect to the clean (111) surface, which is negative [$\gamma = (N_{thiol}E_b + E_{rec})/A)/(eV·Å^{-2})$].
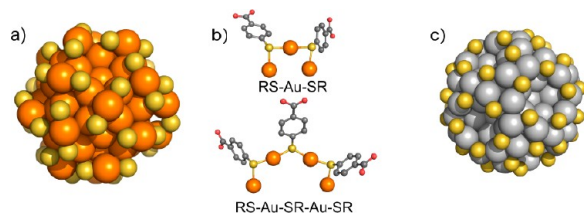
Figure 6. (a) $Au_{102}(MBA)_{44}$ cluster. (b) Two kinds of staple motifs found on the Au cluster surface. Coordinates obtained from O. Lopez-Acevedo (ref 90). (c) $Ag_{92}(AgSR)_{60}{}^{2+}$ cluster.[91] Orange: Au; yellow: S; light gray: Ag; dark gray: C; red: O. For clarity, only the S head of the thiol molecules is shown in the clusters in (a) and (c).

has been the elucidation of the $Au_{102}(MBA)_{44}$ crystal structure by X-ray diffraction[86] (Figure 6a). The core of this thiolate–AuNC has been found to be packed in a Marks decahedron (a neutral 79-atom Au core), surrounded by two types of "staple" motifs (RS-Au_{ad}-SR and RS-Au_{ad}-RS-Au_{ad}-SR, Figure 6b). In these complexes, the central Au atom is linearly coordinated by surface-parallel bonds to the two thiolates, bridging two Au atoms underneath of the first surface layer, and sulfur atoms occupy Au on-top sites. In order to understand the stability of these clusters, two distinct approaches have been proposed. On one hand is the superatom model with a closed electron-shell structure based on global electronic effects,[87] where the Au_{ad} is present as Au(I). In this model, the staple is also stabilized by long-range "aurophilic" Au–Au coordination. On the other hand, a model based on thermodynamical considerations and strong local chemical effects has been proposed. In this case, the S atom retains the thyil form, and the Au_{ad} remains as Au(0).[88] Finally, it is interesting to stress that the thiol coverage is $\theta = 0.7$, much higher than $\theta = 0.25$ for MBA on Au(111).[34] Geometry optimization and ab initio molecular dynamics have shown that staple formation is preferred because it stabilizes the cluster by pinning the surface Au atoms.[89]

The presence of the staple motif was later verified on different thiolate-protected AuNCs by X-ray diffraction[92] and X-ray absorption data.[93,94] The thiol capping seems to play a role in the thermodynamic and electrochemical stability of thiol–AuNC.[95] In general, aliphatic thiols have higher electrochemical and thermodynamic stability than aromatic thiols, in agreement with data for the Au(111) (Table 1 and Figure 5).

In contrast to AuNCs, the scarcity of reports on AgNCs may be assigned to the high reactivity and poor stability of the Ag(SR) interface. However, some progress in this direction has been recently made. In fact, a superatom complex with a molecular formula $Ag_{44}(SR)_{30}{}^{4-}$ has been synthesized.[96] In a similar way, 2 nm size AgNCs have also been prepared by reduction of a silver thiolate precursor, $Ag(SCH_2CH_2Ph)$.[91] In this case, a core–shell structure model was developed, with a 92-atom Ag core having icosahedral–dodecahedral symmetry and an encapsulating protective shell containing Ag atoms and 60 thiolates arranged in a network of six-membered rings resembling the geometry found in alkanethiolate SAMs on Ag(111)[97] (Figure 6c). On the other hand, it has been shown that glutathione-capped Ag_{25} clusters decompose at 50 °C, yielding Ag_2S NPs 3 nm in diameter.[98]

Regarding $Pd_n(SR)_m$ clusters, these have been prepared by reactions between palladium chloride and alkanethiols.[99] The size of the clusters (which are in the range of $5 < n < 60$, $m \approx 0.6n$) is consistent with the ~1 nm core diameters observed by TEM. For instance, the $[Pd(SC_{12}H_{25})_2]_6$ complex

has six palladium atoms, forming a nearly planar hexagonal ring with the adjacent Pd atoms bridged by sulfur atoms from both sides.[100] However, as the size of the metallic Pd core is increased, marked changes in the structure and chemistry take place.[101] Thus, PdNCs, 1.2 nm in size, capped with different alkanethiols (number of C atoms = 12, 16, and 18) show evidence of PdS_x in the bulk.

The previous discussion demonstrates a strong correlation regarding surface structure and chemistry between thiolate-protected NCs and SAMs on (111) surfaces.

Thiolate-Protected NPs. The structure of thiolate-protected AuNPs has been studied from both experimental and theoretical viewpoints. (DT)-protected AuNPs (5−8 nm in size) have been analyzed by high-resolution TEM (HRTEM) and theoretically modeled.[34] Careful examination of the images shows that about 1/3 of the particles either contain a single twin plane or are decahedral. The remaining 2/3 are single fcc NPs, some of which appear "spherical" in shape, while others exhibit faceting, as predicted by recent DFT calculations.[102] Most of them can be described in terms of the truncated octahedral motif with the crystal surface dominated by {111} (77%) and {100} (23%) planes.[34]

Concerning surface chemistry, some evidence about the presence of RS-Au_{ad}-SR on the {111} face of 300 nm diameter gold nanocrystals results from recent coherent X-ray diffraction measurements.[103] Upon thiol self-assembly, the flat facets contract radially inward relative to its spherical regions. The magnitude and slow kinetics of the contraction are consistent with the formation of a RS-Au_{ad}-SR layer. Theoretical and experimental data indicates the existence of RS-Au_{ad} species and increased surface disorder upon thiol adsorption,[104] although a vacancy island cannot be formed on the {111} facets of small AuNPs (Figure 4b).

Typical HRTEM images obtained for DT (prepared by BS-II method) and MBA (prepared by BS-I method) monolayer-protected AuNPs with average sizes ranging from 2 to 3 nm are shown in Figure 7a,b. In the above discussion, it was stated that
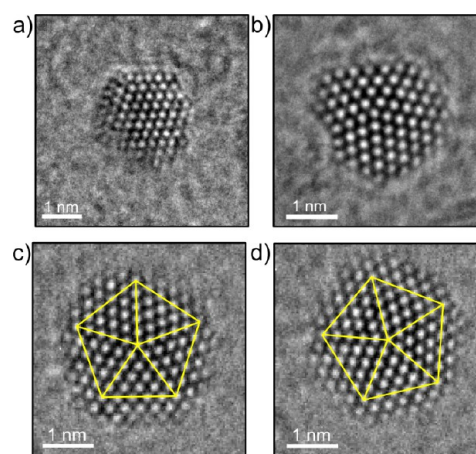
Figure 7. a) DT-protected AuNPs prepared by the two-phase Brust–Schiffrin method supported on amorphous carbon. (b) MBA-protected AuNPs prepared by the one-phase Brust–Schiffrin method. (c,d) Two HRTEM images of the same MBA-protected AuNP. The electron beam produces not only the rotation of the NP but also the displacements of the atoms closer to the surface of the NPs. In smaller NPs, this effect is also important for inner atoms. The lines were drawn for reference. Images taken with a Philips CM300FEG/UT microscope at NCEM, Berkeley.
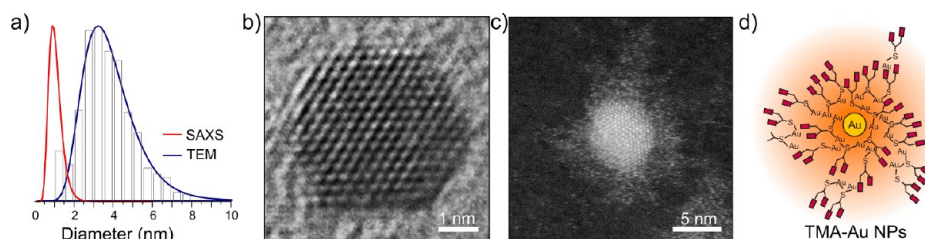
Figure 8. TMA-protected AuNPs. (a) SAXS versus TEM size distribution (adapted from ref 107), (b) HRTEM image (adapted from ref 24), (c) high-angle annular dark field scanning TEM (HAADF-STEM) image (obtained with a JEOL JEM-ARM200F by G. Casillas, UTSA, U.S.A.), and (d) schematic drawing of the NP structure.

thiolate-protected AuNPs approach their expected thermodynamic shape and that their surface chemistry is consistent with RS-Au$_{ad}$-SR species. However, marked changes in both structure and chemistry of AuNPs have been observed under HRTEM imaging and X-ray characterization. In fact, NPs illuminated by an intense electron beam are damaged due to atom ionization, breaking bonds, local heating, and knock-on displacements[31] (Figure 7c,d).

The electron beam can result not only in changes in the position of the atoms in the NPs, evident by comparing the images in Figure 7 c and d, but also in dramatic changes in surface chemistry. For example, TMA-protected AuNCs appear ~1 nm in size when characterized by small-angle X-ray scattering (SAXS) (Figure 8a) but transform into ~3 nm AuNPs in size under HRTEM imaging (Figure 8a,b). This results from the reduction of the Au(I) polymeric species that surround the Au core to Au(0), as revealed by HAADF-STEM (Figure 8c) and schematically shown in Figure 8d. In fact, a synthetic method for AgNPs (2−6 nm in size) based on the reduction of RS-Ag by electron beam irradiation has been described.[105] On the other hand, DT-Ni(II) complexes are not reduced under similar imaging conditions.[27] Radiation damage during X-ray absorption experiments on alkanethiolate-capped AuNPs has been also observed after 45 min of exposure, resulting in S−C bond cleavage and atomic S formation.[106]

The high surface free energy (and strain) of the small NP and NC surfaces also plays a key role in surface chemistry. In fact, while MBA SAMs show no evidence of surface reconstruction on Au(111) terraces[54] (Figure 5), the situation is very different on the {111} facets of small NPs (<3 nm in size) because their 4−5% lattice contraction[43,45] should enhance vacancy (adatom) formation upon thiol adsorption (Figure 4c). We have estimated that the reconstruction energy per MBA (E_{rec}/N_{thiol}) to form RS-Au$_{ad}$-RS moieties decreases from 0.555 (Figure 5) to 0.539 eV when the Au−Au distance decreases 5%, that is, the formation of this species on the strained surface is favored. Also, the defective sites (Figure 4) at the NP's surface provide Au$_{ad}$ for staple formation. After adsorption, the bonds created by thiol molecules with adatom/surface atoms release the excess surface free energy, and thiolate-protected Au[24,108,109] exhibits a surface lattice expansion.[86] The higher thiol coverage ($\theta = 2/3$) found for AuNPs <4 nm in size with respect to Au(111) ($\theta = 1/3$) results from the NP curvature and larger ligand/Au binding ratios on core edges and vertexes.[110] These effects vanish for AuNPs >4 nm, and θ approaches 1/3.[111] In contrast, a slight lattice expansion has been observed for thiolate-protected PdNPs[18] due to H incorporation during NP synthesis or sulfide formation.[112]

Thiol adsorption is also accompanied by changes in the NPs' electronic properties. XPS measurements showed that thiolate adsorption induces a positive binding energy (BE) shift in the

> **Electrons and X-rays can induce dramatic changes in NP structure and surface chemistry.**

Au 4f core level.[113] The valence band exhibited small BE shifts, which were interpreted as rehybridization of Au 5d electrons due to the Au−S bond formation. Furthermore, the disappearance of the Fermi edge upon thiol adsorption, which was attributed to a sulfur-induced metal−insulator transition of the NP, was observed. Similar results were reported for AgNPs. However, different phenomena, such as final-state effects, were proposed to explain Au 4f BE shifts in thiolate-protected AuNPs.[114] The difficulty to uncouple these effects makes the analysis of the BE shifts more difficult. However, the shift in the Pd 3d signal in PdNPs is much higher than that for the 4f signal of AuNPs because of the presence of PdS$_x$ on the surface (Figure 9a). The valence band spectrum of AuNPs is located at a greater BE than
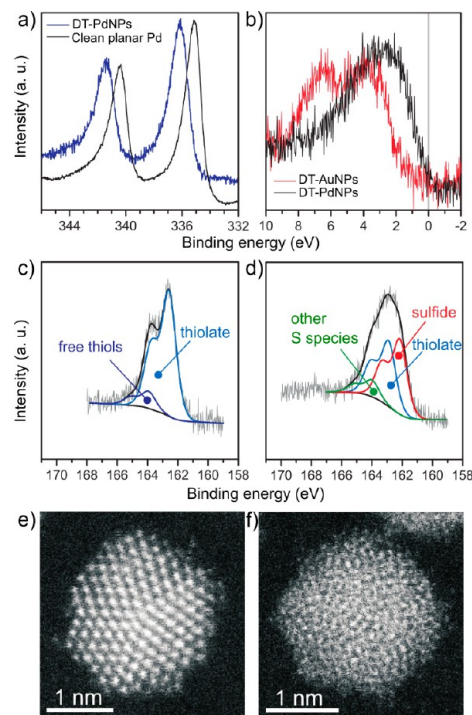
Figure 9. (a) Comparison of the Pd 3d spectrum of DT-protected PdNPs and a clean planar Pd surface. (b) Valence band signal of DT-protected Pd and Au NPs. (c) S 2p spectrum of DT-protected AuNPs. (d) S 2p spectrum of DT-protected PdNPs. (e,f) HAADF-STEM images of alkylamine-protected PdNPs and alkanethiolate-protected PdNPs, respectively. Adapted from ref 18.

the one of PdNPs (Figure 9b), a fact closely related to the high reactivity of Pd compared to Au.[18] Regarding the S 2p signal, it evidences the already commented differences in the chemistry of thiolate-protected Pd and Au NPs. In AuNPs, the signal can be deconvoluted into two components, the main one at ∼162.5 eV, assigned to the thiolate monolayer, and a smaller one at ∼163.5 eV, assigned to free thiol (Figure 9c). In the case of PdNPs, the total amount of S is about twice that found in AuNPs of a similar size, thus revealing the presence of sulfides. In this case, three components are necessary to fit the signal. The two main components at 162 and 163 eV have been assigned to sulfide and thiolate, respectively, while a minor component at higher binding energy has been assigned to different oxidized S species (Figure 9d).[18]

The strong influence of the sulfide layer on the PdNPs structure is evident in high-resolution HAADF-STEM images. While amine-protected PdNPs are crystalline (Figure 9e), thiolate-protected PdNPs are amorphous (Figure 9f), a result that can be related to the presence of the PdS_x layer. In fact, the synthesis at $T = -78$ °C results in crystalline PdNPs,[22] suggesting that the formation of the sulfide layer is kinetically hindered at low T. On the other hand, Pd(II)-SR complexes are used as precursors to prepare thiolate-protected PdS_x NPs through high-temperature-induced decomposition,[115] that is, C−S bond cleavage is favored at high T. Concerning thiolates, DFT calculations on Pd(111) suggest that the sulfide-covered PdNP surface could contain RS-Pd_{ad}-SR species,[60] as in the case of Au(111) surfaces and AuNCs.

Also for AgNPs, a core−shell morphology consisting of a metallic Ag core surrounded by a Ag_2S-like phase has been proposed.[116] The increase in the thiol concentration leads to smaller AgNPs and produces more Ag_2S.[116] Therefore, the proposed structure for AgNPs resembles that described for thiolate-protected PdNPs. However, XPS data for DT-protected AgNPs synthesized in our laboratory by the BS-II method showed only a small amount of sulfide, which is not consistent with thiolates grafted on a Ag@Ag_2S core@shell model. Also, thermogravimetric analysis data for thiolate-protected AgNPs prepared by the BS-I method showed no evidence of an excess of S in relation to that for intact thiol molecules.[21] However, DFT calculations for a hypothetical $(\sqrt{7} \times \sqrt{7})R19.1°$ sulfur + thiol on Ag(111) (similar to that shown for Pd in Figure 3d) yields $\gamma = -0.148$ eV/Å^2, a value very close to $\gamma = -0.154$ eV/Å^2 calculated for thiolate SAMs on the reconstructed Ag(111) (Table 1). Therefore, thiolate-protected AgNPs and thiolate-protected Ag@Ag_2S core@shell NPs have a similar stability, and the final product could depend on details of the synthetic procedure[117] or on the presence of sulfides impurities.[118] In fact, Ag(I) thiolates react rapidly with H_2S or HS$^-$ to form Ag_2S,[119] and then, thiols can bind the silver sulfide, leading to thiolate-protected Ag@Ag_2S core@shell NPs.[120]

In conclusion, we have discussed the surface chemistry of thiolate-protected Au, Pd, and AgNPs, an important issue in relation to applications in many technological fields. We have shown that there is a correlation between the surface chemistry of these NPs and those found in the corresponding (111) extended surfaces. Metal thiolates play a dominant role in the {111} faces of AuNPs, while both thiolates and sulfides are present on PdNPs and on AgNPs, although for different reasons, the intrinsic catalytic activity of Pd and the sensitivity of AgNP to preparation conditions. Surface reconstruction of {111} NP facets upon thiol adsorption is enhanced in relation

> Metal thiolates play a dominant role in the {111} faces of AuNPs, while both thiolates and sulfides are present on PdNPs and on AgNPs, although for different reasons, the intrinsic catalytic activity of Pd and the sensitivity of AgNP to preparation conditions.

to that of plain surfaces due to bond contraction and a large number of defects, both favoring vacancy/adatom formation. On the basis of some experimental and DFT data thiol adsorption would not induce reconstruction of {100} Au and Ag faces of NPs.

Future work in the subject should address several important topics. For instance, our knowledge on the surface chemistry and structure of thiolates at surface defects should be improved as they become increasingly important as the NP size decreases. Also, much more experimental data are needed on thiol adsorption on the {100} faces because their contribution to the total NP surface increases with the NP size. Both topics become crucial in order to link extended surfaces with NP surfaces. Moreover, more information about S−C bond cleavage is necessary, in particular, on the role of defects in this process and on the effect of adsorbed sulfide to promote strong disorder in the NPs' cores. Finally, it would be important to have a better understanding of the impact of electrons and X-rays on the surface chemistry and structure as this seems to induce uncontrolled changes on the surface chemistry and structure of NPs.

■ AUTHOR INFORMATION

Corresponding Author
*E-mail: robsalva@inifta.unlp.edu.ar; Fax: +54 221 425 4642; Phone: +54 221 425 7430; Web: http://nano.quimica.unlp.edu.ar.

Present Address
#G.C.: Max Planck Research Department for Structural Dynamics, Center for Free Electron Laser Science, University of Hamburg, Luruper Chaussee 149, 22761 Hamburg, Germany.

Author Contributions
⊥J.C.A. and G.C. contributed equally to this work.

Notes
The authors declare no competing financial interest.

Biographies

Julio C. Azcárate received his degree in Chemistry from the National University of La Plata (UNLP) in 2009. He is currently a Ph.D. student at the Research Institute of Theoretical and Applied Chemistry (INIFTA), UNLP, Argentina.

Gastón Corthey received his Ph.D. in Chemistry from UNLP in 2012, and he is currently a postdoctoral fellow at the Max Planck Research Department for Structural Dynamics, University of Hamburg, Germany.

Evangelina Pensa received her degree in Chemistry from UNLP in 2009. She is currently a Ph.D. student at INIFTA.

Carolina Vericat received her Ph.D. from UNLP (2003). She is Adjoint Researcher of CONICET at INIFTA and Professor of Chemistry at UNLP.

Mariano H. Fonticelli received his Ph.D. from UNLP (2002). He is Independent Researcher of CONICET at INIFTA and Professor of Physical Chemistry at UNLP.

Roberto C. Salvarezza received his Ph.D. from the University of Buenos Aires, Argentina (1981). He is Superior Researcher of CONICET and head of the SPM and Surface Physical Chemistry Group.

Pilar Carro received her Ph.D. from La Laguna University (ULL), Spain (1986). She is Research Member of The Institute of Materials and Nanotechnology of La Laguna University and Professor of Physical Chemistry at ULL.

■ REFERENCES

(1) De, M.; Ghosh, P. S.; Rotello, V. M. Applications of Nanoparticles in Biology. *Adv. Mater.* **2008**, *20*, 4225−4241.

(2) Minelli, C.; Lowe, S. B.; Stevens, M. M. Nanomedicine: Engineering Nanocomposite Materials for Cancer Therapy. *Small* **2010**, *6*, 2336−2357.

(3) Jin, R. The Impacts of Nanotechnology on Catalysis by Precious Metal Nanoparticles. *Nanotech. Rev.* **2012**, *1*, 31−55.

(4) Barnes, W. L.; Dereux, A.; Ebbesen, T. W. Surface Plasmon Subwavelength Optics. *Nature* **2003**, *424*, 824−830.

(5) Talapin, D. V.; Lee, J.-S.; Kovalenko, M. V.; Shevchenko, E. V. Prospects of Colloidal Nanocrystals for Electronic and Optoelectronic Applications. *Chem. Rev.* **2009**, *110*, 389−458.

(6) Love, J. C.; Estroff, L. A.; Kriebel, J. K.; Nuzzo, R. G.; Whitesides, G. M. Self-Assembled Monolayers of Thiolates on Metals as a Form of Nanotechnology. *Chem. Rev.* **2005**, *105*, 1103−1170.

(7) Sperling, R. A.; Parak, W. J. Surface Modification, Functionalization and Bioconjugation of Colloidal Inorganic Nanoparticles. *Philos. Trans. R. Soc. London, Ser. A* **2010**, *368*, 1333−1383.

(8) Brust, M.; Fink, J.; Bethell, D.; Schiffrin, D. J.; Kiely, C. Synthesis and Reactions of Functionalised Gold Nanoparticles. *J. Chem. Soc., Chem. Commun.* **1995**, *16*, 1655−1656.

(9) Brust, M.; Walker, M.; Bethell, D.; Schiffrin, D. J.; Whyman, R. Synthesis of Thiol-Derivatised Gold Nanoparticles in a Two-Phase Liquid−Liquid System. *J. Chem. Soc., Chem. Commun.* **1994**, *7*, 801−802.

(10) He, S.; Yao, J.; Jiang, P.; Shi, D.; Zhang, H.; Xie, S.; Pang, S.; Gao, H. Formation of Silver Nanoparticles and Self-Assembled Two-Dimensional Ordered Superlattice. *Langmuir* **2001**, *17*, 1571−1575.

(11) Li, Y.; Zaluzhna, O.; Xu, B.; Gao, Y.; Modest, J. M.; Tong, Y. J. Mechanistic Insights into the Brust−Schiffrin Two-Phase Synthesis of Organo-chalcogenate-Protected Metal Nanoparticles. *J. Am. Chem. Soc.* **2011**, *133*, 2092−2095.

(12) Zamborini, F. P.; Gross, S. M.; Murray, R. W. Synthesis, Characterization, Reactivity, and Electrochemistry of Palladium Monolayer Protected Clusters. *Langmuir* **2000**, *17*, 481−488.

(13) Castro, E. G.; Salvatierra, R. V.; Schreiner, W. H.; Oliveira, M. M.; Zarbin, A. J. G. Dodecanethiol-Stabilized Platinum Nanoparticles Obtained by a Two-Phase Method: Synthesis, Characterization, Mechanism of Formation, and Electrocatalytic Properties. *Chem. Mater.* **2009**, *22*, 360−370.

(14) Templeton, A. C.; Wuelfing, W. P.; Murray, R. W. Monolayer-Protected Cluster Molecules. *Acc. Chem. Res.* **1999**, *33*, 27−36.

(15) Zhu, L.; Zhang, C.; Guo, C.; Wang, X.; Sun, P.; Zhou, D.; Chen, W.; Xue, G. New Insight into Intermediate Precursors of Brust−Schiffrin Gold Nanoparticles Synthesis. *J. Phys. Chem. C* **2013**, *117*, 11399−11404.

(16) Goulet, P. J. G.; Lennox, R. B. New Insights into Brust−Schiffrin Metal Nanoparticle Synthesis. *J. Am. Chem. Soc.* **2010**, *132*, 9582−9584.

(17) Branham, M. R.; Douglas, A. D.; Mills, A. J.; Tracy, J. B.; White, P. S.; Murray, R. W. Arylthiolate-Protected Silver Quantum Dots. *Langmuir* **2006**, *22*, 11376−11383.

(18) Corthey, G.; Rubert, A. A.; Picone, A. L.; Casillas, G.; Giovanetti, L. J.; Ramallo-López, J. M.; Zelaya, E.; Benitez, G. A.; Requejo, F. G.; José-Yacamán, M.; et al. New Insights into the Chemistry of Thiolate-Protected Palladium Nanoparticles. *J. Phys. Chem. C* **2012**, *116*, 9830−9837.

(19) Jose, D.; Matthiesen, J. E.; Parsons, C.; Sorensen, C. M.; Klabunde, K. J. Size Focusing of Nanoparticles by Thermodynamic Control through Ligand Interactions. Molecular Clusters Compared with Nanoparticles of Metals. *J. Phys. Chem. Lett.* **2012**, *3*, 885−890.

(20) Dhanalakshmi, L.; Udayabhaskararao, T.; Pradeep, T. Conversion of Double Layer Charge-Stabilized Ag@Citrate Colloids to Thiol Passivated Luminescent Quantum Clusters. *Chem. Commun.* **2012**, *48*, 859−861.

(21) Farrag, M.; Thämer, M.; Tschurl, M.; Bürgi, T.; Heiz, U. Preparation and Spectroscopic Properties of Monolayer-Protected Silver Nanoclusters. *J. Phys. Chem. C* **2012**, *116*, 8034−8043.

(22) Cargnello, M.; Wieder, N. L.; Canton, P.; Montini, T.; Giambastiani, G.; Benedetti, A.; Gorte, R. J.; Fornasiero, P. A. Versatile Approach to the Synthesis of Functionalized Thiol-Protected Palladium Nanoparticles. *Chem. Mater.* **2011**, *23*, 3961−3969.

(23) Ackerson, C. J.; Jadzinsky, P. D.; Kornberg, R. D. Thiolate Ligands for Synthesis of Water-Soluble Gold Clusters. *J. Am. Chem. Soc.* **2005**, *127*, 6550−6551.

(24) Corthey, G.; Giovanetti, L. J.; Ramallo-López, J. M.; Zelaya, E.; Rubert, A. A.; Benitez, G. A.; Requejo, F. G.; Fonticelli, M. H.; Salvarezza, R. C. Synthesis and Characterization of Gold@Gold(I)-Thiomalate Core@Shell Nanoparticles. *ACS Nano* **2010**, *4*, 3413−3421.

(25) Le Guével, X.; Trouillet, V.; Spies, C.; Jung, G.; Schneider, M. Synthesis of Yellow-Emitting Platinum Nanoclusters by Ligand Etching. *J. Phys. Chem. C* **2012**, *116*, 6047−6051.

(26) Lei, S.-B.; Wang, C.; Yin, S.-X.; Wan, L.-J.; Bai, C.-L. Assembling Nanometer Nickel Particles into Ordered Arrays. *ChemPhysChem* **2003**, *4*, 1114−1117.

(27) Calderón, M. F.; Zelaya, E.; Benitez, G. A.; Schilardi, P. L.; Creus, A. H.; Orive, A. G.; Salvarezza, R. C.; Ibañez, F. J. New Findings for the Composition and Structure of Ni Nanoparticles Protected with Organomercaptan Molecules. *Langmuir* **2013**, *29*, 4670−4678.

(28) Shon, Y.-S.; Gross, S. M.; Dawson, B.; Porter, M.; Murray, R. W. Alkanethiolate-Protected Gold Clusters Generated from Sodium S-Dodecylthiosulfate (Bunte Salts). *Langmuir* **2000**, *16*, 6555−6561.

(29) Shon, Y.-S.; Cutler, E. Aqueous Synthesis of Alkanethiolate-Protected Ag Nanoparticles Using Bunte Salts. *Langmuir* **2004**, *20*, 6626−6630.

(30) Mari, A.; Imperatori, P.; Marchegiani, G.; Pilloni, L.; Mezzi, A.; Kaciulis, S.; Cannas, C.; Meneghini, C.; Mobilio, S.; Suber, L. High Yield Synthesis of Pure Alkanethiolate-Capped Silver Nanoparticles. *Langmuir* **2010**, *26*, 15561−15566.

3135

dx.doi.org/10.1021/jz401526y | *J. Phys. Chem. Lett.* 2013, 4, 3127−3138

(31) Wang, Z. L. Transmission Electron Microscopy of Shape-Controlled Nanocrystals and Their Assemblies. *J. Phys. Chem. B* **2000**, *104*, 1153−1175.

(32) Tao, A. R.; Habas, S.; Yang, P. Shape Control of Colloidal Metal Nanocrystals. *Small* **2008**, *4*, 310−325.

(33) Frenken, J. W. M.; Stoltze, P. Are Vicinal Metal Surfaces Stable? *Phys. Rev. Lett.* **1999**, *82*, 3500−3503.

(34) Barnard, A. S.; Lin, X. M.; Curtiss, L. A. Equilibrium Morphology of Face-Centered Cubic Gold Nanoparticles >3 nm and the Shape Changes Induced by Temperature. *J. Phys. Chem. B* **2005**, *109*, 24465−24472.

(35) Barnard, A. S.; Young, N. P.; Kirkland, A. I.; van Huis, M. A.; Xu, H. Nanogold: A Quantitative Phase Map. *ACS Nano* **2009**, *3*, 1431−1436.

(36) Cleveland, C. L.; Landman, U.; Schaaff, T. G.; Shafigullin, M. N.; Stephens, P. W.; Whetten, R. L. Structural Evolution of Smaller Gold Nanocrystals: The Truncated Decahedral Motif. *Phys. Rev. Lett.* **1997**, *79*, 1873−1876.

(37) Barnard, A. S. Mapping the Shape and Phase of Palladium Nanocatalysts. *Catal. Sci. Technol.* **2012**, *2*, 1485−1492.

(38) Wang, B.; Liu, M.; Wang, Y.; Chen, X. Structures and Energetics of Silver and Gold Nanoparticles. *J. Phys. Chem. C* **2011**, *115*, 11374−11381.

(39) Casillas, G.; Velázquez-Salazar, J. J.; Jose-Yacaman, M. A New Mechanism of Stabilization of Large Decahedral Nanoparticles. *J. Phys. Chem. C* **2012**, *116*, 8844−8848.

(40) Quan, Z.; Wang, Y.; Fang, J. High-Index Faceted Noble Metal Nanocrystals. *Acc. Chem. Res.* **2013**, *46*, 191−202.

(41) Page, K.; Proffen, T.; Terrones, H.; Terrones, M.; Lee, L.; Yang, Y.; Stemmer, S.; Seshadri, R.; Cheetham, A. K. Direct Observation of the Structure of Gold Nanoparticles by Total Scattering Powder Neutron Diffraction. *Chem. Phys. Lett.* **2004**, *393*, 385−388.

(42) Vermaak, J. S.; Mays, C. W.; Kuhlmann-Wilsdorf, D. On Surface Stress and Surface Tension: I. Theoretical Considerations. *Surf. Sci.* **1968**, *12*, 128−133.

(43) Szczerba, W.; Riesemeier, H.; Thünemann, A. Bond Length Contraction in Gold Nanoparticles. *Anal. Bioanal. Chem.* **2010**, *398*, 1967−1972.

(44) Qi, W.; Huang, B.; Wang, M. Bond-Length and Energy Variation of Small Gold Nanoparticles. *J. Comput. Theor. Nanosci.* **2009**, *6*, 635−639.

(45) Mamatkulov, M.; Filhol, J.-S. Intrinsic Electrochemical and Strain Effects in Nanoparticles. *J. Phys. Chem. C* **2013**, *117*, 2334−2343.

(46) Nanda, K. K.; Maisels, A.; Kruis, F. E. Surface Tension and Sintering of Free Gold Nanoparticles. *J. Phys. Chem. C* **2008**, *112*, 13488−13491.

(47) Vericat, C.; Vela, M. E.; Benitez, G.; Carro, P.; Salvarezza, R. C. Self-Assembled Monolayers of Thiols and Dithiols on Gold: New Challenges for a Well-Known System. *Chem. Soc. Rev.* **2010**, *39*, 1805−1834.

(48) Tang, L.; Li, F.; Zhou, W.; Guo, Q. The Structure of Methylthiolate and Ethylthiolate Monolayers on Au(111): Absence of the $(\sqrt{3}\times\sqrt{3})R30°$ Phase. *Surf. Sci.* **2012**, *606*, L31−L35.

(49) Pensa, E.; Cortés, E.; Corthey, G.; Carro, P.; Vericat, C.; Fonticelli, M. H.; Benítez, G.; Rubert, A. A.; Salvarezza, R. C. The Chemistry of the Sulfur−Gold Interface: In Search of a Unified Model. *Acc. Chem. Res.* **2012**, *45*, 1183−1192.

(50) Maksymovych, P.; Sorescu, D. C.; Yates, J. T., Jr. Gold-Adatom-Mediated Bonding in Self-Assembled Short-Chain Alkanethiolate Species on the Au(111) Surface. *Phys. Rev. Lett.* **2006**, *97*, 146103.

(51) Maksymovych, P.; Sorescu, D. C.; Voznyy, O.; Yates, J. T. Hybridization of Phenylthiolate- and Methylthiolate-Adatom Species at Low Coverage on the Au(111) Surface. *J. Am. Chem. Soc.* **2013**, *135*, 4922−4925.

(52) Kautz, N. A.; Kandel, S. A. Alkanethiol/Au(111) Self-Assembled Monolayers Contain Gold Adatoms: Scanning Tunneling Microscopy before and after Reaction with Atomic Hydrogen. *J. Am. Chem. Soc.* **2008**, *130*, 6908−6909.

(53) Carro, P.; Torres, D.; Diaz, R.; Salvarezza, R. C.; Illas, F. Mechanisms of Defect Generation and Clustering in CH₃S Self-Assembled Monolayers on Au(111). *J. Phys. Chem. Lett.* **2012**, *3*, 2159−2163.

(54) Pensa, E.; Rubert, A. A.; Benitez, G.; Carro, P.; González Orive, A.; Hernández Creus, A.; Salvarezza, R. C.; Vericat, C. Are 4-Mercaptobenzoic Acid Self Assembled Monolayers on Au(111) a Suitable System to Test Adatom Models? *J. Phys. Chem. C* **2012**, *116*, 25765−25771.

(55) Pensa, E.; Carro, P.; Rubert, A. A.; Benítez, G.; Vericat, C.; Salvarezza, R. C. Thiol with an Unusual Adsorption−Desorption Behavior: 6-Mercaptopurine on Au(111). *Langmuir* **2010**, *26*, 17068−17074.

(56) Dubois, L. H.; Zegarski, B. R.; Nuzzo, R. G. Molecular Ordering of Organosulfur Compounds on Au(111) and Au(100): Adsorption from Solution and in Ultrahigh Vacuum. *J. Chem. Phys.* **1993**, *98*, 678−688.

(57) Schweizer, M.; Hagenström, H.; Kolb, D. M. Potential-Induced Structure Transitions in Self-Assembled Monolayers: Ethanethiol on Au(100). *Surf. Sci.* **2001**, *490*, L627−L636.

(58) Love, J. C.; Wolfe, D. B.; Haasch, R.; Chabinyc, M. L.; Paul, K. E.; Whitesides, G. M.; Nuzzo, R. G. Formation and Structure of Self-Assembled Monolayers of Alkanethiolates on Palladium. *J. Am. Chem. Soc.* **2003**, *125*, 2597−2609.

(59) Corthey, G.; Rubert, A. A.; Benitez, G. A.; Fonticelli, M. H.; Salvarezza, R. C. Electrochemical and X-ray Photoelectron Spectroscopy Characterization of Alkanethiols Adsorbed on Palladium Surfaces. *J. Phys. Chem. C* **2009**, *113*, 6735−6742.

(60) Carro, P.; Corthey, G.; Rubert, A. A.; Benitez, G. A.; Fonticelli, M. H.; Salvarezza, R. C. The Complex Thiol−Palladium Interface: A Theoretical and Experimental Study. *Langmuir* **2010**, *26*, 14655−14662.

(61) Ramírez, E. A.; Cortés, E.; Rubert, A. A.; Carro, P.; Benítez, G.; Vela, M. E.; Salvarezza, R. C. Complex Surface Chemistry of 4-Mercaptopyridine Self-Assembled Monolayers on Au(111). *Langmuir* **2012**, *28*, 6839−6847.

(62) Fischer, J. A.; Zoldan, V. C.; Benitez, G.; Rubert, A. A.; Ramirez, E. A.; Carro, P.; Salvarezza, R. C.; Pasa, A. A.; Vela, M. E. Sulfidization of Au(111) from Thioacetic Acid: An Experimental and Theoretical Study. *Langmuir* **2012**, *28*, 15278−15285.

(63) Wirde, M.; Gelius, U.; Nyholm, L. Self-Assembled Monolayers of Cystamine and Cysteamine on Gold Studied by XPS and Voltammetry. *Langmuir* **1999**, *15*, 6370−6378.

(64) Houmam, A.; Muhammad, H.; Koczkur, K. M. Rapid Formation of a Dense Sulfur Layer on Gold through Use of Triphenylmethane Sulfenyl Chloride as a Precursor. *Langmuir* **2012**, *28*, 16881−16889.

(65) Mann, F. G.; Purdie, D. The Constitution of Complex Metallic Salts. Part III. The Parachors of Palladium and Mercury in Simple and Complex Compounds. *J. Chem. Soc.* **1935**, 1549−1563.

(66) Laibinis, P. E.; Whitesides, G. M.; Allara, D. L.; Tao, Y. T.; Parikh, A. N.; Nuzzo, R. G. Comparison of the Structures and Wetting Properties of Self-Assembled Monolayers of *n*-Alkanethiols on the Coinage Metal Surfaces, Copper, Silver, and Gold. *J. Am. Chem. Soc.* **1991**, *113*, 7152−7167.

(67) Rong, H.-T.; Frey, S.; Yang, Y.-J.; Zharnikov, M.; Buck, M.; Wühn, M.; Wöll, C.; Helmchen, G. On the Importance of the Headgroup Substrate Bond in Thiol Monolayers: A Study of Biphenyl-Based Thiols on Gold and Silver. *Langmuir* **2001**, *17*, 1582−1593.

(68) Yu, M.; Woodruff, D. P.; Satterley, C. J.; Jones, R. G.; Dhanak, V. R. Structure of the Pentylthiolate Self-Assembled Monolayer on Ag(111). *J. Phys. Chem. C* **2007**, *111*, 10040−10048.

(69) Yu, M.; Driver, S. M.; Woodruff, D. P. Scanning Tunneling Microscopy Investigation of the Structure of Methanethiolate on Ag(111). *Langmuir* **2005**, *21*, 7285−7291.

(70) Torres, D.; Carro, P.; Salvarezza, R. C.; Illas, F. Evidence for the Formation of Different Energetically Similar Atomic Structures in Ag(111)-$(\sqrt{7}\times\sqrt{7})$-R19.1°-CH₃S. *Phys. Rev. Lett.* **2006**, *97*, 226103.

(71) Abufager, P. N.; Alvarez Soria, L.; Martiarena, M. L.; Reuter, K.; Busnengo, H. F. Structure of the Methylthiolate Monolayer on

3136

dx.doi.org/10.1021/jz401526y | *J. Phys. Chem. Lett.* 2013, 4, 3127−3138

Ag(111): The Role of Substrate Vacancies. *Chem. Phys. Lett.* **2011**, *503*, 71–74.

(72) Fenter, P.; Eisenberger, P.; Li, J.; Camillone, N.; Bernasek, S.; Scoles, G.; Ramanarayanan, T. A.; Liang, K. S. Structure of Octadecyl Thiol Self-Assembled on the Silver(111) Surface: an Incommensurate Monolayer. *Langmuir* **1991**, *7*, 2013–2016.

(73) Hu, L.; de la Rama, L. P.; Efremov, M. Y.; Anahory, Y.; Schiettekatte, F.; Allen, L. H. Synthesis and Characterization of Single-Layer Silver-Decanethiolate Lamellar Crystals. *J. Am. Chem. Soc.* **2011**, *133*, 4367–4376.

(74) Rodríguez, L. M.; Gayone, J. E.; Sánchez, E. A.; Grizzi, O.; Blum, B.; Salvarezza, R. C. Room-Temperature Kinetics of Short-Chain Alkanethiol Film Growth on Ag(111) from the Vapor Phase. *J. Phys. Chem. B* **2006**, *110*, 7095–7097.

(75) Lewis, M.; Tarlov, M.; Carron, K. Study of the Photooxidation Process of Self-Assembled Alkanethiol Monolayers. *J. Am. Chem. Soc.* **1995**, *117*, 9574–9575.

(76) Kondoh, H.; Tsukabayashi, H.; Yokoyama, T.; Ohta, T. S. K-edge X-ray Absorption Fine Structure Study of Vacuum-Deposited Dihexyldisulfide on Ag(100). *Surf. Sci.* **2001**, *489*, 20–28.

(77) Alloway, D. M.; Graham, A. L.; Yang, X.; Mudalige, A.; Colorado, R.; Wysocki, V. H.; Pemberton, J. E.; Randall Lee, T.; Wysocki, R. J.; Armstrong, N. R. Tuning the Effective Work Function of Gold and Silver Using ω-Functionalized Alkanethiols: Varying Surface Composition through Dilution and Choice of Terminal Groups. *J. Phys. Chem. C* **2009**, *113*, 20328–20334.

(78) Grönbeck, H.; Häkkinen, H.; Whetten, R. L. Gold-Thiolate Complexes Form a Unique c(4 × 2) Structure on Au(111). *J. Phys. Chem. C* **2008**, *112*, 15940–15942.

(79) Zheng, J.; Nicovich, P. R.; Dickson, R. M. Highly Fluorescent Noble-Metal Quantum Dots. *Annu. Rev. Phys. Chem.* **2007**, *58*, 409–431.

(80) Cathcart, N.; Mistry, P.; Makra, C.; Pietrobon, B.; Coombs, N.; Jelokhani-Niaraki, M.; Kitaev, V. Chiral Thiol-Stabilized Silver Nanoclusters with Well-Resolved Optical Transitions Synthesized by a Facile Etching Procedure in Aqueous Solutions. *Langmuir* **2009**, *25*, 5840–5846.

(81) Santiago González, B.; Rodríguez, M. J.; Blanco, C.; Rivas, J.; López-Quintela, M. A.; Martinho, J. M. G. One Step Synthesis of the Smallest Photoluminescent and Paramagnetic PVP-Protected Gold Atomic Clusters. *Nano Lett.* **2010**, *10*, 4217–4221.

(82) Crooks, R. M.; Zhao, M.; Sun, L.; Chechik, V.; Yeung, L. K. Dendrimer-Encapsulated Metal Nanoparticles: Synthesis, Characterization, and Applications to Catalysis. *Acc. Chem. Res.* **2000**, *34*, 181–190.

(83) Wei, H.; Wang, Z.; Yang, L.; Tian, S.; Hou, C.; Lu, Y. Lysozyme-Stabilized Gold Fluorescent Cluster: Synthesis and Application as Hg^{2+} Sensor. *Analyst* **2010**, *135*, 1406–1410.

(84) Geddes, C. D.; Parfenov, A.; Gryczynski, I.; Lakowicz, J. R. Luminescent Blinking from Silver Nanostructures. *J. Phys. Chem. B* **2003**, *107*, 9989–9993.

(85) Shang, L.; Dong, S.; Nienhaus, G. U. Ultra-Small Fluorescent Metal Nanoclusters: Synthesis and Biological Applications. *Nano Today* **2011**, *6*, 401–418.

(86) Jadzinsky, P. D.; Calero, G.; Ackerson, C. J.; Bushnell, D. A.; Kornberg, R. D. Structure of a Thiol Monolayer-Protected Gold Nanoparticle at 1.1 Å Resolution. *Science* **2007**, *318*, 430–433.

(87) Häkkinen, H. The Gold–Sulfur Interface at the Nanoscale. *Nat. Chem.* **2012**, *4*, 443–455.

(88) Reimers, J. R.; Wang, Y.; Cankurtaran, B. O.; Ford, M. J. Chemical Analysis of the Superatom Model for Sulfur-Stabilized Gold Nanoparticles. *J. Am. Chem. Soc.* **2010**, *132*, 8378–8384.

(89) Jiang, D.-e.; Tiago, M. L.; Luo, W.; Dai, S. The "Staple" Motif: A Key to Stability of Thiolate-Protected Gold Nanoclusters. *J. Am. Chem. Soc.* **2008**, *130*, 2777–2779.

(90) Walter, M.; Akola, J.; Lopez-Acevedo, O.; Jadzinsky, P. D.; Calero, G.; Ackerson, C. J.; Whetten, R. L.; Grönbeck, H.; Häkkinen, H. A Unified View of Ligand-Protected Gold Clusters as Superatom Complexes. *Proc. Natl. Acad. Sci. U.S.A.* **2008**, *105*, 9157–9162.

(91) Chakraborty, I.; Govindarajan, A.; Erusappan, J.; Ghosh, A.; Pradeep, T.; Yoon, B.; Whetten, R. L.; Landman, U. The Superstable 25 kDa Monolayer Protected Silver Nanoparticle: Measurements and Interpretation as an Icosahedral Ag$_{152}$(SCH$_2$CH$_2$Ph)$_{60}$ Cluster. *Nano Lett.* **2012**, *12*, 5861–5866.

(92) Heaven, M. W.; Dass, A.; White, P. S.; Holt, K. M.; Murray, R. W. Crystal Structure of the Gold Nanoparticle [N(C$_8$H$_{17}$)$_4$][Au$_{25}$(SCH$_2$CH$_2$Ph)$_{18}$]. *J. Am. Chem. Soc.* **2008**, *130*, 3754–3755.

(93) MacDonald, M. A.; Zhang, P.; Qian, H.; Jin, R. Site-Specific and Size-Dependent Bonding of Compositionally Precise Gold-Thiolate Nanoparticles from X-ray Spectroscopy. *J. Phys. Chem. Lett.* **2010**, *1*, 1821–1825.

(94) Stellwagen, D.; Weber, A.; Bovenkamp, G. L.; Jin, R.; Bitter, J. H.; Kumar, C. S. S. R. Ligand Control in Thiol Stabilized Au$_{38}$ Clusters. *RSC Adv.* **2012**, *2*, 2276–2283.

(95) Jung, J.; Kang, S.; Han, Y.-K. Ligand Effects on the Stability of Thiol-Stabilized Gold Nanoclusters: Au$_{25}$(SR)$_{18}^-$, Au$_{38}$(SR)$_{24}$, and Au$_{102}$(SR)$_{44}$. *Nanoscale* **2012**, *4*, 4206–4210.

(96) Harkness, K. M.; Tang, Y.; Dass, A.; Pan, J.; Kothalawala, N.; Reddy, V. J.; Cliffel, D. E.; Demeler, B.; Stellacci, F.; Bakr, O. M.; McLean, J. A. Ag$_{44}$(SR)$_{30}^{4-}$: A Silver-Thiolate Superatom Complex. *Nanoscale* **2012**, *4*, 4269–4274.

(97) Yu, M.; Woodruff, D. P.; Bovet, N.; Satterley, C. J.; Lovelock, K.; Jones, R. G.; Dhanak, V. Structure Investigation of Ag(111) ($\sqrt{7}\times\sqrt{7}$)R19°-SCH$_3$ by X-ray Standing Waves: A Case of Thiol-Induced Substrate Reconstruction. *J. Phys. Chem. B* **2006**, *110*, 2164–2170.

(98) Remya, K. P.; Udayabhaskararao, T.; Pradeep, T. Low-Temperature Thermal Dissociation of Ag Quantum Clusters in Solution and Formation of Monodisperse Ag$_2$S Nanoparticles. *J. Phys. Chem. C* **2012**, *116*, 26019–26026.

(99) Negishi, Y.; Murayama, H.; Tsukuda, T. Formation of Pd$_n$(SR)$_m$ Clusters (n < 60) in the Reactions of PdCl$_2$ and RSH (R = n-C$_{18}$H$_{37}$, n-C$_{12}$H$_{25}$). *Chem. Phys. Lett.* **2002**, *366*, 561–566.

(100) Yang, Z.; Smetana, A. B.; Sorensen, C. M.; Klabunde, K. J. Synthesis and Characterization of a New Tiara Pd(II) Thiolate Complex, [Pd(SC$_{12}$H$_{25}$)$_2$]$_6$, and Its Solution-Phase Thermolysis to Prepare Nearly Monodisperse Palladium Sulfide Nanoparticles. *Inorg. Chem.* **2007**, *46*, 2427–2431.

(101) Ramallo-López, J. M.; Giovanetti, L.; Craievich, A. F.; Vicentin, F. C.; Marín-Almazo, M.; José-Yacaman, M.; Requejo, F. G. XAFS, SAXS and HREM Characterization of Pd Nanoparticles Capped with n-Alkyl Thiol Molecules. *Physica B* **2007**, *389*, 150–154.

(102) Barmparis, G. D.; Honkala, K.; Remediakis, I. N. Thiolate Adsorption on Au(hkl) and Equilibrium Shape of Large Thiolate-Covered Gold Nanoparticles. *J. Chem. Phys.* **2013**, *138*, 064702/1–064702/9.

(103) Watari, M.; McKendry, R. A.; Vögtli, M.; Aeppli, G.; Soh, Y.-A.; Shi, X.; Xiong, G.; Huang, X.; Harder, R.; Robinson, I. K. Differential Stress Induced by Thiol Adsorption on Facetted Nanocrystals. *Nat. Mater.* **2011**, *10*, 862–866.

(104) Mariscal, M. M.; Olmos-Asar, J. A.; Gutierrez-Wing, C.; Mayoral, A.; Yacaman, M. J. On the Atomic Structure of Thiol-Protected Gold Nanoparticles: A Combined Experimental and Theoretical Study. *Phys. Chem. Chem. Phys.* **2010**, *12*, 11785–11790.

(105) Kim, S.-E.; Kim, J.-U.; Han, Y. H.; Lee, B. C.; Lee, J.-C. Size Controlled Miniscale Synthesis of Silver Nanoparticles Using TEM Electron Beam. *J. Nanosci. Nanotechnol.* **2008**, *8*, 5212–5215.

(106) Ramallo-López, J. M.; Giovanetti, L. J.; Vicentin, F. C.; Requejo, F. G. XANES Study of the Radiation Damage on Alkanethiolates-Capped Au Nanoparticles. *J. Phys.: Conf. Ser.* **2013**, *430*, 012034.

(107) Corthey, G.; Giovanetti, L. J.; Ramallo-López, J. M.; Zelaya, E.; Rubert, A. A.; Benitez, G. A.; Requejo, F. G.; Fonticelli, M. H.; Salvarezza, R. C. Synthesis and Characterization of Gold@Gold(I)-Thiomalate Core@ Shell Nanoparticles. *LNLS Activity Report* **2010**, 10–15.

(108) Menard, L. D.; Xu, H.; Gao, S.-P.; Twesten, R. D.; Harper, A. S.; Song, Y.; Wang, G.; Douglas, A. D.; Yang, J. C.; Frenkel, A. I.; et al.

3137

dx.doi.org/10.1021/jz401526y | *J. Phys. Chem. Lett.* 2013, 4, 3127–3138

Metal Core Bonding Motifs of Monodisperse Icosahedral Au$_{13}$ and Larger Au Monolayer-Protected Clusters As Revealed by X-ray Absorption Spectroscopy and Transmission Electron Microscopy. *J. Phys. Chem. B* **2006**, *110*, 14564−14573.

(109) Zanchet, D.; Tolentino, H.; Martins Alves, M. C.; Alves, O. L.; Ugarte, D. Inter-Atomic Distance Contraction in Thiol-Passivated Gold Nanoparticles. *Chem. Phys. Lett.* **2000**, *323*, 167−172.

(110) Hostetler, M. J.; Wingate, J. E.; Zhong, C.-J.; Harris, J. E.; Vachet, R. W.; Clark, M. R.; Londono, J. D.; Green, S. J.; Stokes, J. J.; Wignall, G. D.; et al. Alkanethiolate Gold Cluster Molecules with Core Diameters from 1.5 to 5.2 nm: Core and Monolayer Properties as a Function of Core Size. *Langmuir* **1998**, *14*, 17−30.

(111) Hinterwirth, H.; Kappel, S.; Waitz, T.; Prohaska, T.; Lindner, W.; Lämmerhofer, M. Quantifying Thiol Ligand Density of Self-Assembled Monolayers on Gold Nanoparticles by Inductively Coupled Plasma-Mass Spectrometry. *ACS Nano* **2013**, *7*, 1129−1136.

(112) Sun, Y.; Frenkel, A. I.; Isseroff, R.; Shonbrun, C.; Forman, M.; Shin, K.; Koga, T.; White, H.; Zhang, L.; Zhu, Y.; et al. Characterization of Palladium Nanoparticles by Using X-ray Reflectivity, EXAFS, and Electron Microscopy. *Langmuir* **2005**, *22*, 807−816.

(113) Büttner, M.; Kröger, H.; Gerhards, I.; Mathys, D.; Oelhafen, P. Changes in the Electronic Structure of Gold Particles upon Thiol Adsorption as a Function of the Mean Particle Size. *Thin Solid Films* **2006**, *495*, 180−185.

(114) Moriarty, P. Comment on "X-Ray Studies of the Structure and Electronic Behavior of Alkanethiolate-Capped Gold Nanoparticles: The Interplay of Size and Surface Effects". *Phys. Rev. Lett.* **2004**, *92*, 109601.

(115) Yang, Z.; Klabunde, K. J.; Sorensen, C. M. From Monodisperse Sulfurized Palladium Nanoparticles to Tiara Pd(II) Thiolate Clusters: Influence of Thiol Ligand on Thermal Treatment of a Palladium(II)-Amine System. *J. Phys. Chem. C* **2007**, *111*, 18143−18147.

(116) Padmos, J. D.; Zhang, P. Surface Structure of Organosulfur Stabilized Silver Nanoparticles Studied with X-ray Absorption Spectroscopy. *J. Phys. Chem. C* **2012**, *116*, 23094−23101.

(117) Oliveira, M. M.; Ugarte, D.; Zanchet, D.; Zarbin, A. J. G. Influence of Synthetic Parameters on the Size, Structure, and Stability of Dodecanethiol-Stabilized Silver Nanoparticles. *J. Colloid Interface Sci.* **2005**, *292*, 429−435.

(118) Zhong, C.-J.; Brush, R. C.; Anderegg, J.; Porter, M. D. Organosulfur Monolayers at Gold Surfaces: Reexamination of the Case for Sulfide Adsorption and Implications to the Formation of Monolayers from Thiols and Disulfides. *Langmuir* **1998**, *15*, 518−525.

(119) Bell, R. A.; Kramer, J. R. Structural Chemistry and Geochemistry of Silver−Sulfur Compounds: Critical Review. *Environ. Toxicol. Chem.* **1999**, *18*, 9−22.

(120) Motte, L.; Pileni, M. P. Self-Assemblies of Silver Sulfide Nanocrystals: Influence of Length of Thio-Alkyl Chains Used as Coating Agent. *Appl. Surf. Sci.* **2000**, *164*, 60−67.

3138

dx.doi.org/10.1021/jz401526y | *J. Phys. Chem. Lett.* 2013, 4, 3127−3138